Threading a Linear Molecule Through a Macrocycle Thanks to Boron: Optical Properties of the Threaded Species and Synthesis of a Rotaxane

Ludmilla Verrieux, Olivier Mongin, Thierry Roisnel, Fabienne Berrée, Arnaud Fihey, Boris Le Guennic, Yann Trolez, Matthieu Hicguet

Threading a Linear Molecule Through a Macrocycle Thanks to Boron: Optical Properties of the Threaded Species and Synthesis of a Rotaxane

Matthieu Hicguet,[a] Ludmilla Verrieux,[a] Olivier Mongin,[a] Thierry Roisnel,[a] Fabienne Berrée,*[a] Arnaud Fihey,*[a] Boris Le Guennic,[a] Yann Trolez*[a]

[a] Matthieu Hicguet, Dr. Ludmilla Verrieux, Prof. Dr. Olivier Mongin, Dr. Thierry Roisnel, Dr. Fabienne Berrée,* Dr. Arnaud Fihey,* Dr. Boris Le Guennic, Dr. Yann Trolez*
Univ Rennes, École Nationale Supérieure de Chimie de Rennes, CNRS, ISCR (Institut des Sciences Chimiques de Rennes) - UMR6226, F-35000 Rennes, France

Abstract: Two BODIPYs and one boron β-diketonate were threaded through a macrocycle bearing a 2,2'-biphenol unit, showing thus the ability of boron to act as a gathering atom. The new threaded species were characterized by 1D and 2D NMR spectroscopy as well as by X-ray crystallography for one of them and their properties rationalized with quantum chemistry to unravel the vibronic contributions. The BODIPYs exhibited interesting fluorescence features with quantum yields up to 91% and enhanced photostability compared to their non-threaded homologues. A rotaxane was synthesized using this threading strategy after stoppering and removing the boron with potassium hydroxide.

Introduction

Threading a linear molecule through a macrocycle has attracted a lot of interest over the last decades.[1] Apart from the seminal works of Wasserman,[2] Schill[3] and Harrison[4] in the 60's where they used statistical threading to end up with the formation of catenanes and rotaxanes, a real breakthrough in this field was published in 1983 with the first reported high-yield threading by the group of Jean-Pierre Sauvage to finally isolate a Cu(I)-catenane after cyclization.[5] The threading relied on the use of copper(I). Each compound containing a 1,10-phenanthroline ligand, the Cu(I) center adopted a tetrahedral geometry, which arranged both ligands in the optimal fashion to subsequently perform a macrocyclization of the thread in order to afford the first Cu(I)-catenane. Since then, numerous strategies were employed to thread molecules through macrocycles with different kinds of interactions at play to gather molecules, from strong interactions (e.g. coordination[6] or covalent bonds[7]) to weak interactions (e.g. hydrogen bonding,[8] π-stacking,[9] anion binding[10] or radical-radical interactions[11]).

To the best of our knowledge, while boron is largely used in synthetic chemistry,[12] interactions with boron have never been used so far to thread a molecule through a macrocycle. Organoboron compounds have been used for long for their chemical reactivity, hydroboration[13] and Suzuki couplings[14] probably being two paradigmatic examples. But they are also synthesized for their optical properties[15] and the luminescence of boron dipyrromethene (BODIPY) is a striking example of the importance of boron in this field.[16] Apart from the chemical and optical properties, boron has been greatly used in molecular assemblies. Various topologies of molecular species encompassing this atom were described in the literature: macrocycles,[17] cages,[18] (pseudo-)rotaxanes,[19] catenanes,[20] helicates.[21] In these striking examples, the role of the boron atom varied from an active participation to the formation of the assembly to a simple spectator through incorporation in the system afterwards. Surprisingly, while Severin and coworkers used boron to stopper a rotaxane in 2008[19a] (Fig. 1) and very recently Schaufelberger and coworkers took advantage of boron to connect two linear molecules to end up with a rotaxane,[22] there is no example in the literature where boron is used to thread a linear molecule through a macrocycle. The closest example is probably to be credited to Nabeshima group where they used the polarisation of six B-F bonds of three BODIPYs to induce the recognition of cationic threads inside the cavity of a macrocycle,[23] but boron was not directly participating to the templating effect by linking the two elements (Fig. 1). We thought it would be interesting to fill this gap by coordinating a boron to a macrocycle and a thread. In addition, different chemical and physical properties may be expected from threaded species and their counterparts that do not encompass a macrocycle. In this paper, we thus report on the threading of two BODIPYs and a boron diketonate through a macrocycle. One of the resulting species was characterized by X-Ray diffraction, in addition to other techniques. In particular, we showed peculiar optical properties of the threaded BODIPYs over their non-threaded homologs, with photostability and photoluminescence quantum yields (PLQY) significantly improved.

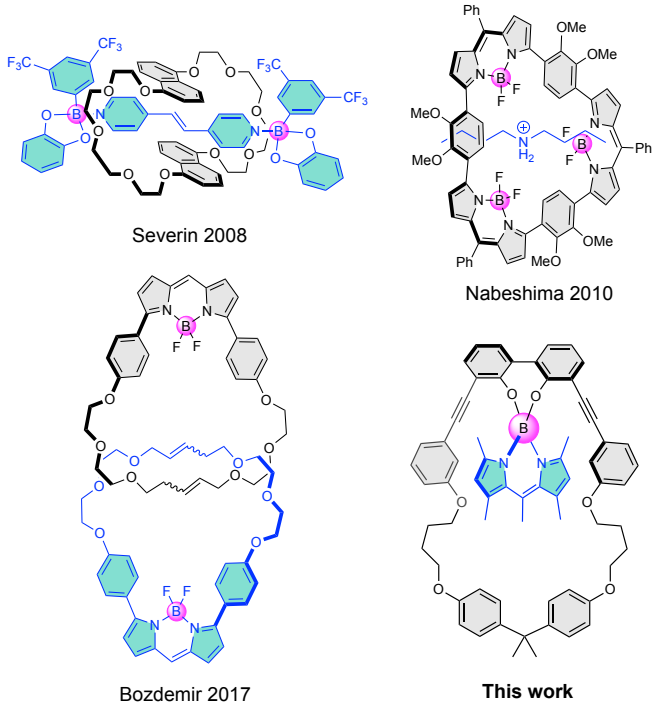

Figure 1. Previously reported interlocked species incorporating boron and this work describing the template effect of boron.

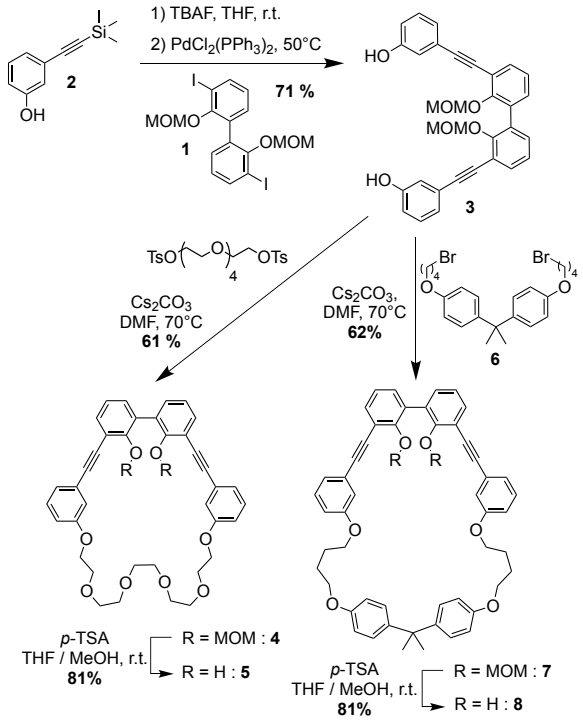

Scheme 1. Synthesis of the two biphenolic macrocycles **5** and **8**.

Results and Discussion

Inspired by the recent works of de La Moya and coworkers who synthesized various BODIPYs substituted with functionalized binols,[24] we designed macrocycles containing a 2,2'-biphenol unit. We started from methoxymethyl (MOM)-protected 2,2'-biphenol **1** bearing two iodines in positions 3 and 3'.[25] It was submitted to a Sonogashira coupling with the meta-trimethylsilylethynylphenol **2**, after in situ deprotection with TBAF, to afford compound **3** in 71% yield (Scheme 1).[26] A macrocyclization between **3** and ditosylated tetraethyleneglycol in highly diluted Williamson conditions led to the isolation of MOM-protected macrocycle **4** in a satisfying 61% yield. Removing the MOMs was achieved using para-toluenesulfonic acid (p-TSA) in 81% yield. The internal cavity of the resulting biphenolic macrocycle **5** was constituted of 32 atoms, with two pending OH groups able to coordinate a boron. A second macrocycle was synthesized by macrocyclization of compound **3** and dibrominated compound **6**[27] to afford a second MOM-protected macrocycle **7** in 62% yield. The MOMs were removed using the same strategy as described before to lead to macrocycle **8** in 81% yield. The internal cavity of the latter is this time constituted of 37 atoms, varying thus the space offered compared with macrocycle **5**.

Then, BODIPY **9** was tentatively threaded through both macrocycles using a reported procedure allowing the substitution of the two fluorines by a 2,2'-biphenol moiety.[28] Thus, this compound was reacted with $AlCl_3$ in anhydrous dichloromethane for 2 hours at reflux and a solution of macrocycle in acetonitrile was then added at room temperature and stirred overnight (Scheme 2). While no threading could be observed with the smallest macrocycle **5**, we isolated product **10** with macrocycle **8** in 31% yield. The same procedure was used with BODIPY **11** and macrocycle **8** to afford compound **12** in 47% yield. In order to explore the generality of this procedure, we used a different substrate: difluoroboron diketonate **13**. In this case, the procedure used was even simpler since compounds **8**, **13** and $AlCl_3$ were mixed all together in dichloromethane. After 15 minutes of stirring at room temperature, compound **14** was isolated in 53% yield. Since the difluoroboron diketonate moiety is significantly smaller than BODIPY **9**, compound **15**[29] (bearing two iodines for potential further functionalization) was tentatively threaded through macrocycle **5**. The corresponding compound **16** was thus isolated in 43% yield, showing thus the importance of the size of the threaded species versus the size of the cavity of the macrocycle. Compounds **10**, **12**, **14** and **16** were characterized by high-resolution mass spectrometry and NMR spectroscopy (see supporting information for more details). For instance, in compound **10**, we observed a strong upfield shift of all the protons belonging to the BODIPY (H-a, H-b, H-c and H-d) by 0.17 to 0.45 ppm (Fig. 2). NOE interactions between these protons and protons 1, 3, 4, 7, 12 and 13 of the macrocycle showed the threaded nature of the assembly (Fig. S14). More generally, several NOE interactions between protons of the macrocycle and the thread were observed in compounds **10**, **12**, **14** and **16** to unambiguously support their structures (Fig. S14, S18, S22 and S26).

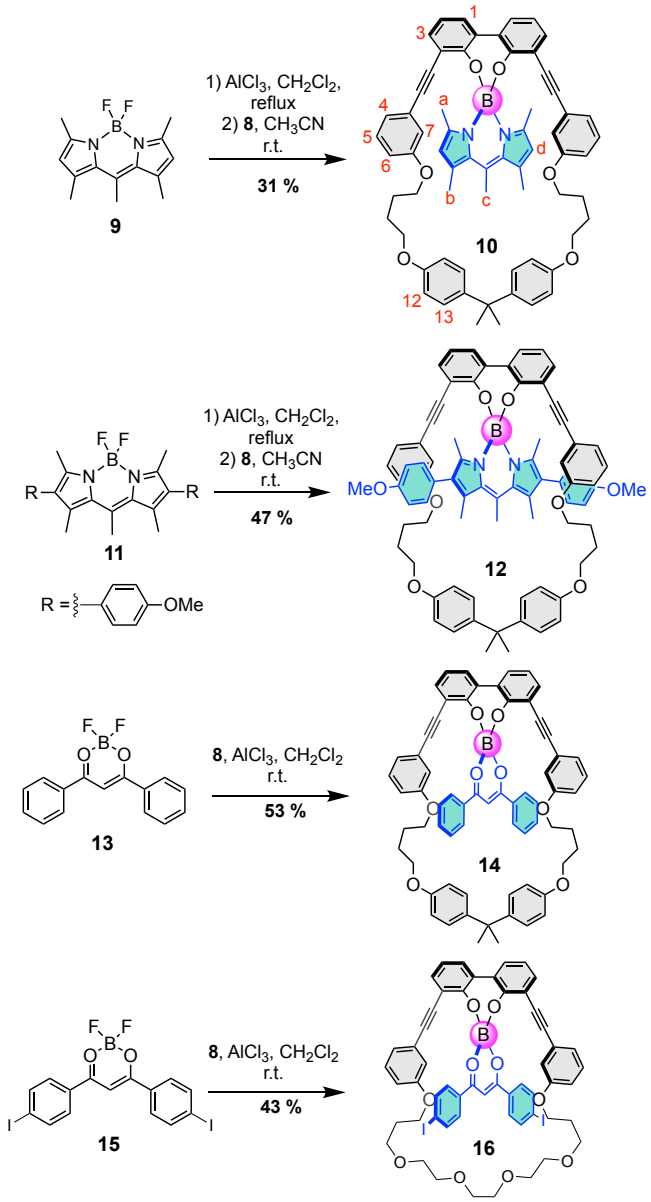

Scheme 2. Threading of compounds **9**, **11**, and **13** inside macrocycle **8** affording threaded compounds **10**, **12**, **14** and **16**.

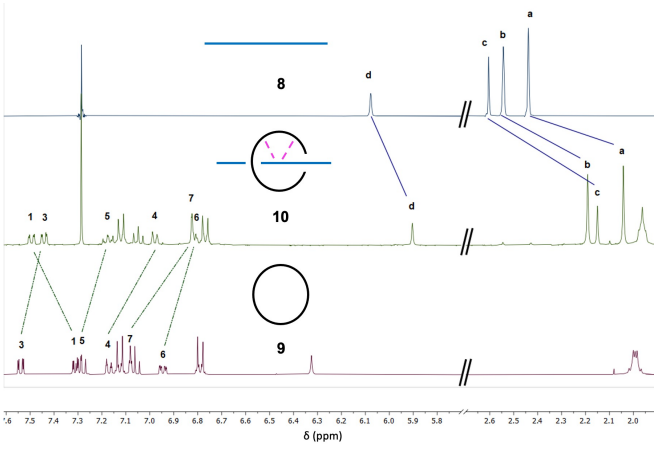

Figure 2. Partial ^{1}H NMR spectra (400 MHz, $CDCl_3$) of a) BODIPY **9**, b) compound **10** and c) macrocycle **8**. The letters and numbers corresponding to the labelling of the protons are shown in Scheme 2.

In addition, single crystals suitable for X-ray diffraction were obtained for compound **10** by slow diffusion of ethanol in a dichloromethane solution. Compound **10** was thus also characterized by X-ray crystallography, definitely confirming that the BODIPY was actually inside the cavity (Fig. 3). Interestingly, the BODIPY is tilted to benefit from supplementary stabilization by π-π interactions with one of the CC triple bonds of the macrocycle (distance: 3.8 Å).

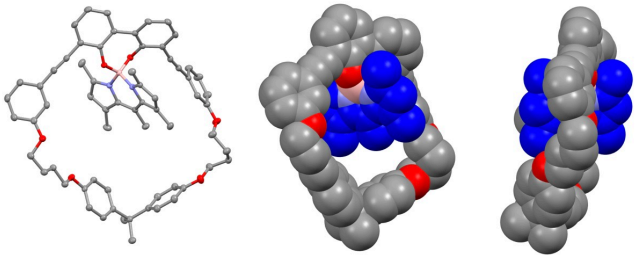

Figure 3. X-Ray structure of compound **10**; solvent molecules and hydrogens were removed for clarity. Left: ellipsoidal representation (50% probability); centre: spacefill representation, face view; right: spacefill representation, lateral view.

The absorption and emission spectra of threaded compounds **10**, **12** and **14** were then recorded. While compound **14** showed no fluorescence, compounds **10** and **12** exhibited usual features of BODIPYs (λ_{abs} = 501 nm and λ_{em} = 516 nm for compound **10**; λ_{abs} = 529 nm and λ_{em} = 578 nm for compound **12**). In particular, we could notice high quantum yields of 91% and 85% respectively in dichloromethane (τ = 6.5 ns and 6.0 ns for **10** and **12**), which means that the presence of the macrocycle around BODIPYs is not detrimental to the fluorescence of the BODIPY. In order to evaluate the impact of this peculiar structure on the emission properties, we synthesized the two corresponding model compounds **17** and **18**, replacing the macrocycle by a simple biphenol (Fig. 4). In this case, while the absorption features are similar to their macrocyclic counterparts **10** and **12** (λ_{abs} = 499 nm for compound **17;** λ_{abs} = 527 nm for compound **18**), we noticed a marked difference of the emission. Actually, the emission of **17** and **18** is slightly red-shifted (λ_{em} = 526 nm and 591 nm respectively) compared to compounds **10** and **12** (Fig. 5 shows the comparison between compounds **10** and **17**). It might seem counter-intuitive at first sight since the overall π -system is smaller but this point is discussed below with the help of TD-DFT calculations. More interestingly, the quantum yields of compounds **17** and **18** are significantly lower (63% and 62% respectively, with τ = 4.6 ns and τ = 5.0 ns), which means that the threaded nature the BODIPYs (at least through macrocycle **8**) largely favors radiative over thermal deactivation. More insights are given by kinetics. While radiative rate constants are very similar in the four systems (around 1.4 x 10^{-8} s^{-1}), non-radiative rate constants are much lower in threaded species **10** and **12** (1.4 x 10^{7} s^{-1} and 2.5 x 10^{7} s^{-1} respectively) than in non-threaded species **17** and **18** (8.0 x 10^{7} s^{-1} and 7.6 x 10^{7} s^{-1} respectively). The macrocycle probably limits movements and vibrations of the BODIPY that allow for thermal deactivation and thus increases the quantum yield. To gain more insights on the structure-properties relationship,[30] another model **19** was synthesized,

which chemical structure is closer to compound **10** but without the macrocycle. Its optical properties are very similar to those of compound **10** with identical absorption and emission maxima (λ_{abs} = 501 nm and λ_{em} = 516 nm) and a quantum yield of 89% (τ = 6.5 ns). Its radiative and non-radiative rate constants are also very similar (1.4 x 10^{-8} s^{-1} and 1.4 x 10^{7} s^{-1} respectively). These observations indicate that the exceptional optical properties of compounds **10** and **12** originate from the structure of the substituted 2,2'-biphenol unit of the macrocycle.

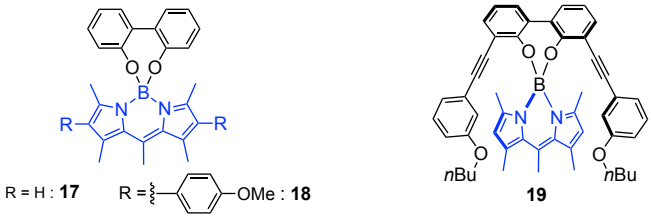

Figure 4. Model compounds **17**-**19**.

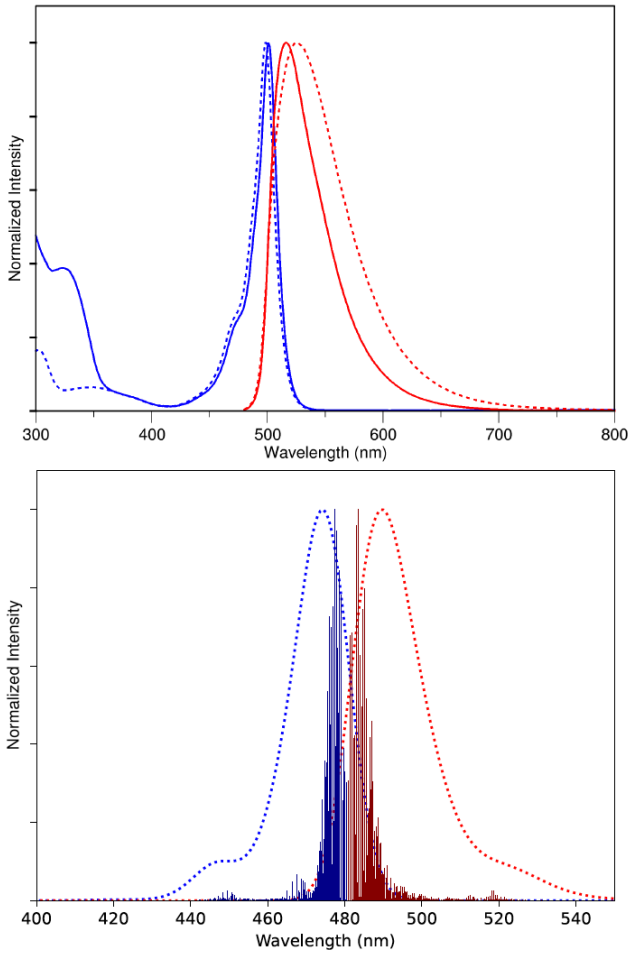

Figure 5. Top: experimental absorption (blue line) and emission (red line) spectra (λ_{ex} = 475 nm) of compounds **10** (solid line) and **17** (dotted line) in dichloromethane. Bottom: computed absorption (blue) and emission (red) vibronic spectra of the first electronic transitions with vibrational transitions (dark blue for absorption and dark red for emission) for compound **17**. For visibility purposes of the vibronic contributions in the first transition, the wavelength rang is restricted in this spectrum to 400-550 nm.

(TD-)DFT calculations have been performed to provide more insights into the spectroscopic and photophysical properties of the series (Tab. 1). Computational details and additional results are provided in the supporting information. First of all, all the structures of **10**, **12**, **17** and **18** were optimized in the ground state (S_0) and then in their first excited state (S_1). The calculated structure of **10** is similar to the crystallographic one (Tab. S2). The computed absorption profiles on optimized geometries of **10**, **12**, **17** and **18**, are dominated by a first intense $S_0 \rightarrow S_1$ electronic transition corresponding to $\pi \rightarrow \pi^*$ excitation between the Highest Occupied Molecular Orbitals (HOMO) and Lowest Unoccupied Molecular Orbitals (LUMO) (Tab. 1 and S3, Fig. S64). The emission band is computed as an intense $S_1 \rightarrow S_0$ electronic transition with the same nature. In contrast, compound **14** presents small oscillator strengths for the computed electronic transitions relative to the absorption and emission (Tab. 1 and S3), easily explained by the lack of overlap between the involved molecular orbitals (see Fig. S64). These observations are in line with the absence of experimental fluorescence. For **10** and **17**, the analysis of the geometry shows that the first exited state presents a small reorganization compared to the ground-state around the boron center (Tab. S2 and Fig. S63). However, compounds **12** and **18** bearing *para*-methoxyphenyl substituents present a difference of dihedral angles between the BODIPY core and the phenyl substituent up to 15° when comparing S_0 and S_1 states (Tab. S2 and Fig. S63). This deformation leads to higher computed shifts between absorption and emission energies for compounds **12** and **18** than for compounds **10** and **17** (Tab. 1), in agreement with experimental observations.

The population analysis shows that the boron center does not contribute to the above mentioned first electronic transition (see Fig. 6 for electronic density difference). The nature of the electronic transition is found to be similar when comparing the isolated and threaded BODIPYs, the electronic densities being located on the core of the BODIPY in both cases. Consequently, the presence of the macrocycle does not induce significant changes on the computed energy of (de)-excitation, for instance when comparing **10** with **17**, or **12** with **18**. Only a very small blue-shift is observed after threading of the BODIPY, in agreement with the spectroscopic measurements, that may be attributed to small changes in the excited-state geometry. In contrast, the addition of -PhOMe groups (**12** and **18**) extends the electronic delocalization in the system (see Fig. 6), leading to a significant red-shift in the computed absorption and emission profiles when comparing to the smaller BODIPY core of **10** and **17**.

	λ_{abs}^{exp} / E_{abs}^{exp}	λ_{em}^{exp} / E_{em}^{exp}	λ_{abs}^{calc} / E_{abs}^{calc}	f_{abs}	λ_{em}^{calc} / E_{em}^{calc}	f_{em}
10	501 / 2.47	516 / 2.40	429 / 2.89	0.40	479 / 2.59	0.58
12	529 / 2.34	578 / 2.15	465 / 2.67	0.61	547 / 2.27	0.71
14	371 / 3.34	-	455 / 2.72	0.01	750 / 1.65	0.004
17	499 / 2.48	526 / 2.36	426 / 2.91	0.45	480 / 2.58	0.67
18	527 / 2.35	591 / 2.10	464 / 2.67	0.70	551 / 2.25	0.75

[a] See the supporting information for additional information and computational details.

Table 1. Experimental and computed absorption and emission properties in dichloromethane.[a] Wavelengths are in nm and energies in eV. Computed oscillator strengths f are also given.

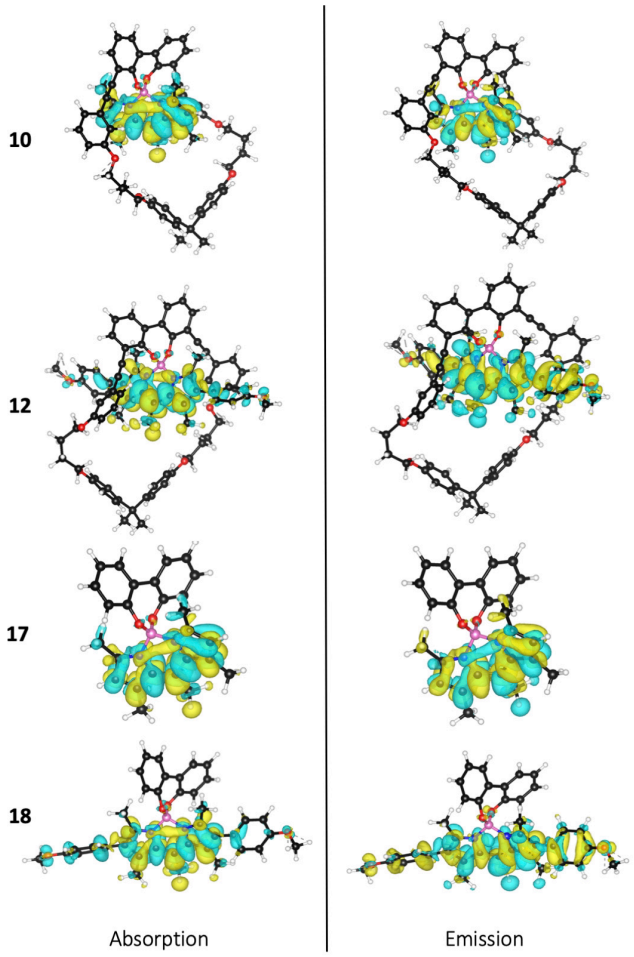

Figure 6. Electronic density difference between the ground and first excited states for absorption (left) and emission (right) (isovalue of 0.0006 a.u.) in dichloromethane. Yellow and blue surfaces represent gain and loss of electronic density, respectively. C, H, B, N, O are in black, white, pink, blue and red, respectively.

The presence of a shoulder in the absorption and emission experimental spectra of **10** and **17** (Fig. 5) can be linked to i) the second electronic transition computed close in energy to the first one (see Tab. S3) or ii) vibrational contributions. Vibronic spectra have been computed for **17** (see Fig. 5) using harmonic approximation (see supporting information for the computational details). Several vibronic transitions with various intensities are found to contribute in the energy region of the experimental shoulder. The nature of the vibrational modes mostly responsible for this band shape corresponds to different deformations between the BODIPY core and the 2,2'-biphenol ligand or localized on the BODIPY core only (see Fig. S65 and animated images).

Within the harmonic approximation, radiative (k_r^{calc}) and internal conversion (k_{ic}^{calc}) rate constants have been computed for the emission process (see supporting information for the computational details). The k_{ic}^{calc} rate constant is in this model the only contribution to the non-radiative rate and is induced by non-adiabatic couplings between the excited and the ground states.[31] The computed rates are listed in Table 2. Regardless of the compound, the computed k_r^{calc} are in the 10^8 s^{-1} range and agree with experimental data. However, the calculation of k_{ic}^{calc} rate constants is more system-dependent. For compounds **10** and **17**, the k_{ic}^{calc} value is similar (≈ 8 x 10^7 s^{-1}, see Tab. 2) and in the same order of magnitude as the k_{nr}^{exp}. The computed value is very close to the measured one for compound **17** (8.6 x 10^7 s^{-1}) but is non-negligibly overestimated for compound **10** (8.3 x 10^7 s^{-1}). As a result, the evolution of the computed quantum yields of fluorescence is not retrieved through vibronic effects, and they are found similar at 66% and 64%. For **12** and **18**, the k_{ic} values differ by an order of magnitude compared to the experimental data. In this case, one can pinpoint the limitation of the harmonic approxtion as these two compounds present a non-negligible reorganization between the two electronic states as described above.[32] The analysis of the Huang-Rhys (HR) factors, which can be associated to the vibronic coupling strength,[33] shows that the main vibrational modes involved in the coupling between the ground and excited states are similar for **10** and **17** (see Fig. S66) and are independent of the choice of the vibronic model. For compound **10**, the presence of the macrocycle actually leads to more modes contributing to the vibronic coupling, but with slightly smaller HR values than in the case of **17** (see Fig. S65 and Fig. S66). From these vibronic computations, the influence of the macrocycle as a facilitator of the radiative pathway cannot be clearly identified. As these calculations are done in a static fashion (one relaxed geometry per state), the impact of threading on the emission of the BODIPY should in principle be studied in a dynamical fashion, to reproduce the population of different conformations at room temperature, which remains non-tractable with the present TD-DFT vibronic models.

COMPOUNDS	k_r^{exp} (s^{-1})	k_{nr}^{exp} (s^{-1})	Φ_F^{exp} (%)	k_r^{calc} (s^{-1})	k_{ic}^{calc} (s^{-1})	Φ_F^{calc} (%)
10	1.4×10^8	1.4×10^7	91	1.5×10^8	8.3×10^7	64
12	1.4×10^8	2.5×10^7	85	1.2×10^8	6.2×10^8	17
17	1.4×10^8	8.0×10^7	63	1.7×10^8	8.6×10^7	66
18	1.2×10^8	7.6×10^7	62	1.3×10^8	8.6×10^8	13

[a] See the supporting information for computational details and additional results.

Table 2. Experimental radiative (k_r^{exp}) and non-radiative (k_{nr}^{exp}) rates constants related to the emission process, compared with computed radiative (k_r^{calc}) and internal conversion (k_{ic}^{calc}) rates constants with a harmonic approximation.[a]

The photostability of compound **10** compared with its model compounds **17 and 19** was evaluated in toluene. To perform this study, a 100 W LED sufficiently powerful was chosen in order to induce the degradation of these compounds in a decent amount of time. More details on the set up are provided in the supporting information. The evolution of each UV-visible spectrum was followed over 8 hours. The absorbance of the main band at the maximum wavelength of each compound as a function of the time of irradiation is provided in Fig. 7. It clearly shows that model compound **17** degraded much quicker than threaded compound **10**. Such enhancement of the photostability of a chromophore inside a macrocycle has already been observed in the past.[34] Compound **19** is more photostable than the other model **17** since it benefits from more steric hindrance around the BODIPY. Nevertheless, while the electronic environment of the BODIPY is exactly the same in compounds **10** and **19**, the threaded compound **10** exhibits a slight but significantly higher photostability than the non-macrocyclic compound **19**. This difference may be attributed to the threaded nature of compound **10** where the BODIPY is even more sterically protected than in model **19**.

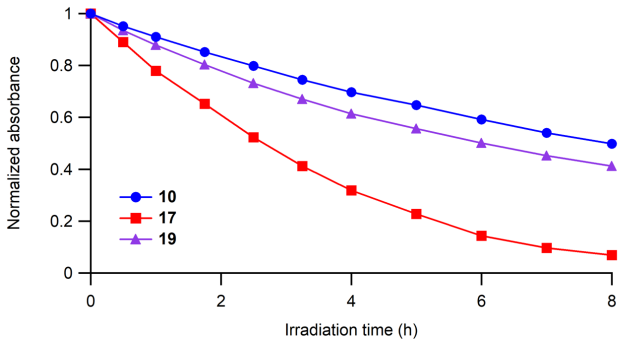

Figure 7. Evolution of the absorbance (normalized at t = 0) upon irradiation of compounds **10**, **17** and **19**.

In order to evaluate the possibility to synthesize a rotaxane using this strategy, we envisaged to stopper a functionalize threaded species like **16** and remove boron, which is known to be sensitive to basic conditions. Since we observed a slight instability of macrocycles **5** and **8** in the course of this project, it was decided to remove their triple bonds and to synthesize another macrocycle using a similar strategy (see ESI for further details). This macrocycle **20** has an internal cavity smaller than **8** but larger than **5**. Compound **15** was thus threaded through macrocycle **20** using the same conditions as above mentioned, affording threaded compound **21** in 38 % yield. The latter was stoppered with a double Sonogashira coupling with acetylenic stopper **22**. [35] Compound **23** was isolated with a very satisfying yield of 88 %. Subsequently, boron was removed from compound **23** in basic conditions in order to end up with the corresponding rotaxane **24** in 45 % yield (Scheme 3). Therefore, this threading strategy with boron proved to be very suitable to the synthesis of new interlocked species.

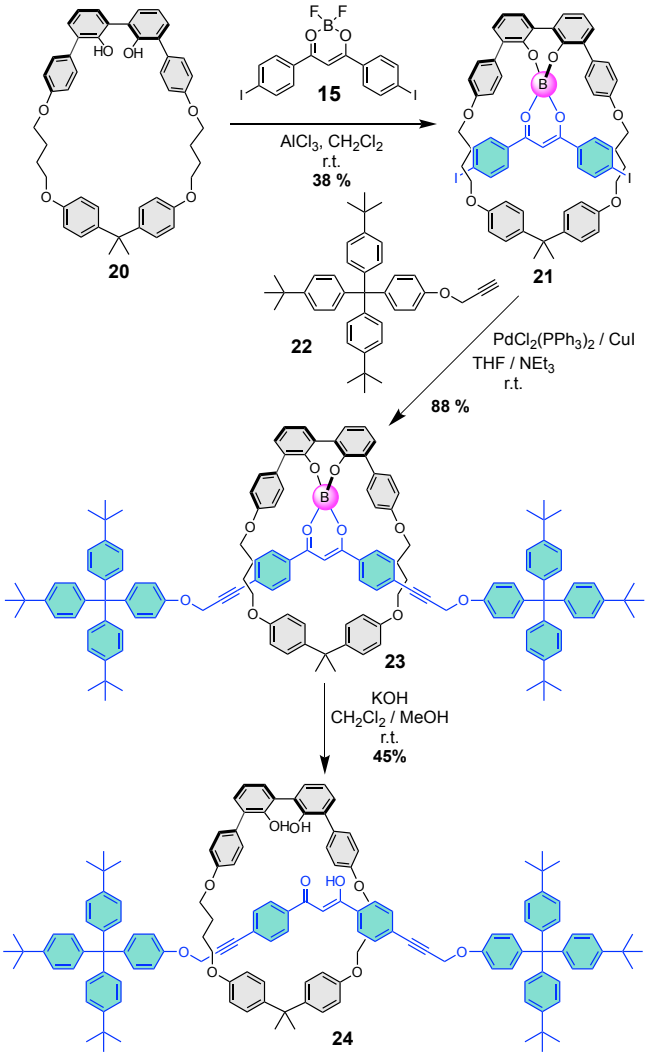

Scheme 3. Synthesis of rotaxane **24**.

Conclusion

We demonstrated that threading may be directed by tetravalent boron in good yields. The threaded BODIPYs showed high quantum yields (85 and 91%), significantly higher than their non-macrocyclic counterparts. In addition, their photostability was greatly improved. These observations show a positive effect of the macrocycle surrounding the BODIPYs, which paves the way to the elaboration of new highly emissive species in the future. In addition, a rotaxane was synthesized in good yields using this threading strategy with boron. This result opens new perspectives in this field by providing a new method to access this kind of compounds. New interlocked species using boron will be investigated in the future.

Supporting Information

The data that support the findings of this study are available in the Supporting Information of this article. Experimental details, including synthetic procedures and characterization data (NMR spectra, UV-vis absorption and fluorescence), additional theoretical results, computational details and crystallographic data.[36]

Acknowledgements

M.H. thanks the University of Rennes for his PhD fellowship. Dr Gregory Pieters from CEA Saclay (France) is acknowledged for fruitful discussions. M.H., F.B. and Y.T. thank the EUR LUMOMAT project and the Investments for the Future program ANR-18-EURE-0012. L.V. acknowledges financial support from Agence Nationale de la Recherche (ANR-21-CE07-0025-03 MAP). L.V., A.F. and B.L.G. thank the French GENCI/IDRIS–CINES center for high–performance computing resources.

Keywords: Boron • Fluorescence • BODIPY • DFT • Rotaxane

[1] For selected reviews: (a) S. Durot, V. Heitz, A. Sour, J.-P. Sauvage, Transition-Metal-Complexed Catenanes and Rotaxanes: From Dynamic Systems to Functional Molecular Machines, edited by Credi A., Silvi S., Venturi M. in *Molecular Machines and Motors: Recent Advances and Perspectives Book series: Current Chemisry*, **2014**, *354*, 35-70. (b) V. Balzani, A. Credi, F. M. Raymo, J. F. Stoddart, *Angew. Chem. Int. Ed.* **2000**, *39*, 3348-3391. (c) J. E. Beves, B. A. Blight, C. J. Campbell, D. A. Leigh, R. T. McBurney, *Angew. Chem. Int. Ed.* **2011**, *50*, 9260-9327. (d) E. M. G. Jamieson, F. Modicom, S. M. Goldup, *Chem. Soc. Rev.* **2018**, *47*, 5266-5311. (e) R. E. Fadler, A. H. Flood, *Front. Chem.* **2022**, *10*, 856173. (f) N. H. Evans, P. D. Beer, *Chem. Soc. Rev.* **2014**, *43*, 4658-4683. (g) J. F. Stoddart, *Angew. Chem. Int. Ed.* **2017**, *56*, 11094-11125. (h) J.-P. Sauvage, *Angew. Chem. Int. Ed.* **2017**, *56*, 11080-11093.

[2] E. Wasserman, *J. Am. Chem. Soc.* **1960**, *82*, 4433-4434.

[3] G. Schill, A. Lüttringhaus, *Angew. Int. Ed.* **1964**, *3*, 546-547.

[4] I. T. Harrison, S. Harrison, *J. Am. Chem. Soc.* **1967**, *89*, 5723-5724.

[5] C. O. Dietrich-Buchecker, J.-P. Sauvage, J.-P. Kintzinger, *Tetrahedron Lett.* **1983**, *24*, 5095-5098.

[6] (a) J. D. Crowley, S. M. Goldup, A.-L. Lee, D. A. Leigh, R. T. McBurney, *Chem. Soc. Rev.* **2009**, *38*, 1530-1541. (b) J.-P. Collin, V. Heitz, J.-P. Sauvage, *Molecular Machines. Topics in Current Chemistry* **2005**, *262*, 29-62. (c) R. Mitra, M. Thiele, F. Octa-Smolin, M. C. Letzel, J. Niemeyer, *Chem. Commun.* **2016**, *52*, 5977-5980. (d) J. H. May, J. M. Van Raden, R. L. Maust, L. N. Zakharov, R. Jasti, *Nature Chem.* **2023**, *15*, 170-176.

[7] (a) C. Schweez, S. Höger, *Chem. Eur. J.* **2018**, *24*, 12006-12009. (b) C. Schweez, P. Shushkov, S. Grimme, S. Höger, *Angew. Chem. Int. Ed.* **2016**, *55*, 3328-3333. (c) Y. Segawa, M. Kuwayama, Y. Hijikata, M. Fushimi, T. Nishihara, J. Pirillo, J. Shirasaki, N. Kubota, K. Itami, *Science* **2019**, *365*, 272-276. (d) A. Bu, Y. Zhao, H. Xiao, C.-H. Tung, L.-Z. Wu, H. Cong, *Angew. Chem. Int. Ed.* **2022**, *61*, e202209449.

[8] C. Reuter, R. Schmieder, F. Vögtle, *Pure Appl. Chem.* **2000**, *72*, 2233-2241.

[9] G. Barin, A. Coskun, M. M. G. Fouda, J. F. Stoddart, *ChemPlusChem* **2012**, *77*, 159-185.

[10] P.D. Beer, M. R. Sambrook, D. Curiel, *Chem. Commun.* **2006**, 2105-2117.

[11] C. J. Bruns, M. Frasconi, J. Iehl, K. J. Hartlieb, S. T. Schneebeli, C. Cheng, S. I. Stupp, J. F. Stoddart, *J. Am. Chem. Soc.* **2014**, *136*, 4714-4723.

[12] For selected reviews on boron chemistry: (a) J. W. B. Fyfe, A. J. B. Watson, *Chem.* **2017**, *3*, 31-55. (b) H. DeFrancesco, J. Dudley, A. Coca, Boron Chemistry: An Overview. In *Boron Reagents in Synthesis. ACS Symposium Series* **2016**, 1-25. (c) Structure, Properties, and Preparation of Boronic Acid Derivatives. Overview of Their Reactions and Applications. In *Boronic Acids: Preparation and Applications in Organic Synthesis and Medicine*; D.G. Hall. (Ed.) Wiley-VCH:Weinheim, Germany, **2005**, 1-134.

[13] For selected reviews: (a) S. Rej, A. Das, T. K. Panda, *Adv. Synth. Catal.* **2021**, *363*, 4818-4840. (b) S. J. Geier, C. M. Vogels, S. A. Westcott, Current Developments in the Catalyzed Hydroboration Reaction. In *Boron Reagents in Synthesis, ACS Symposium Series* **2016**, 209-225. (c) A. G. Karatjas, H. A. McBriarty, S. I. Braye, D. Piscitelli, Synthesis of Pinacolboronates via Hydroboration. In *Boron Reagents in Synthesis. ACS Symposium Series* **2016**, 227-240.

[14] For selected reviews: (a) B. S. Kadu, Suzuki-Miyaura Cross Coupling Reaction: Recent Advancements in Catalysis and Organic Synthesis. *Catal. Sci. Technol.* **2021**, *11*, 1186-1221. (b) A. B. Pagett, G. C. Lloyd-Jones, The Suzuki-Miyaura Cross-Coupling Reaction. In *Organic Reactions*. S. E Denmark (Ed.), Wiley-VCH; **2019**, *100*, 547-620. (c) I. D. Kostas, (Ed.) Suzuki-Miyaura Cross-Coupling Reaction and Potential Applications. In *Catalysts, MDPI*, **2017**, 272 pages. (d) C. Valente, M. G. Organ, The Contemporary Suzuki-Miyaura Reaction. In *Boronic Acids: Preparation and Applications in Organic Synthesis, Medicine and Materials.* Hall, D.G. (Ed.) Wiley-VCH:Weinheim, Germany, **2011**, *1*, 213-262.

[15] C. D. Entwistle, T. B. Marder, *Angew. Chem. Int. Ed.* **2002**, *41*, 2927-2931.

[16] (a) R. Ziessel, G. Ulrich, A. Harriman, *New. J. Chem.* **2007**, *31*, 496-501. (b) R. L. Gapare, A. Thompson, *Chem. Commun*. **2022**, *58*, 7351-7359. (c) R. G. Clarke, M. J. Hall, *Adv. Heterocycl. Chem.* **2019**, *128*, 181-261. (d) Y. V. Zatsikha, Y. P. Kovtun, The Main Strategies of Design and

Applications of BODIPYs. In *Handbook of Porphyrin Science* K. M. Kadish, K. M. Smith, R. Guilard, (Ed.) World Scientific, **2016**, 151-257.

[17] (a) X. Yin, J. Liu, F. Jäkle, *Chem. Eur. J.* **2021**, *27*, 2973-2986. (b) P. M. Mitrasinovic, *Curr. Org. Synth.* **2012**, *9*, 233-246. (c) N. Christinat, R. Scopelliti, K. Severin, *Angew. Chem. Int. Ed.* **2008**, *47*, 1848-1852. (d) K. Ono, S. Onoderab, H. Kawai, *Chem. Commun.* **2022**, *58*, 12544-12547. (e) W. Zhou, T. Sarma, L. Yang, C. Lei, J. L. Sessler, *Chem. Sci.* **2022**, *13*, 7276-7282.

[18] (a) M. Hähsler, M. Mastalerz, *Chem. Eur. J.* **2021**, *27*, 233-237. (b) H. Takata, K. Ono, N. Iwasawa, *Chem. Commun.* **2020**, *56*, 5613.

[19] (a) N. Christinat, R. Scopelliti, K. Severin, *Chem. Commun.* **2008**, 3660-3662. (b) R. Arumugaperumal, V. Srinivasadesikan, M. V. Ramakrishnam Raju, M.-C. Lin, T. Shukla, R. Singh, H.-C. Lin, *ACS Appl. Mater. Interfaces* **2015**, *7*, 26491-26503. (c) Y. Koyama, T. Matsumura, T. Yui, O. Ishitani, T. Takata, *Org. Lett.* **2013**, *15*, 4686-4689. (d) M. Rémy, I. Nierengarten, B. Park, M. Holler, U. Hahn, J.-F. Nierengarten, *Chem. Eur. J.* **2021**, *27*, 8492-8499. (e) Y. Wu, M. Frasconi, W.-G. Liu, R. M. Young, W. A. Goddard III, M. R. Wasielewski, J. F. Stoddart, *J. Am. Chem. Soc.* **2020**, *142*, 11835-11846.

[20] B. Nisanci, S. Sahinoglu, E. Tuner, M. Arik, I. Kani, A. Dastana, Ö. A. Bozdemir, *Chem. Commun.* **2017**, *53*, 12418-12421.

[21] M. Yamamoto, M. Takeuchi, S. Shinkai, *Tetrahedron* **2002**, *58*, 7251-7258. (b) D. Taura, H. Min, C. Katan, E. Yashima, *New J. Chem.* **2015**, *39*, 3259-3269.

[22] J. Yu, M. Gaedke, S. Das, D. L. Stares, C. A. Schalley, F. Schaufelberger, **2023**, ChemRxiv https:///doi.org/10.26434/chemrxiv-2023-v95p8.

[23] (a) N. Sakamoto, C. Ikeda, T. Nabeshima, *Chem. Commun.* **2010**, *46*, 6732-6734. (b) T. Nakamura, G. Yamaguchi, T. Nabeshima, *Angew. Chem. Int. Ed.* **2016**, *55*, 9606-9609.

[24] E. M. Sanchez-Carnerero, F. Moreno, B. L. Maroto, A. R. Agarrabeitia, M. J. Ortiz, B. G. Vo, G. Muller, S. de la Moya, *J. Am. Chem. Soc.* **2014**, *136*, 3346-3349.

[25] K. W. Bentley, L. A. Joyce, E. C. Sherer, H. Sheng, C. Wolf, C. J. Welch, *J. Org. Chem.* **2016**, *81*, 1185-1191.

[26] J.-K. Liu, W. Gu, X.-R. Cheng, J.-P. Cheng, W.-X. Zhou, A.-H. Nie, *Chin. Chem. Lett.* **2015**, *26*, 1327-1330.

[27] F. Durola, J.-P. Sauvage, O. S. Wenger, *Helv. Chim. Acta*, **2007**, *90*, 1439-1446.

[28] C. Tahtaoui, C. Thomas, F. Rohmer, P. Klotz, G. Duportail, Y. Mély, D. Bonnet, M. Hibert, *J. Org. Chem.* **2007**, *72*, 269-27.

[29] R. Yoshii, A. Nagai, K. Tanaka, Y. Chujo, *Macromol. Rapid Commun.* **2014**, *35*, 1315-1319.

[30] J. Jiménes, R. Prieto-Montero, B. L. Maroto, F. Moreno, M. J. Ortiz, A. Oliden-Sánchez, I. López-Arbeloa, V. Martínez-Martínez, S. de la Moya, *Chem. Eur. J.* **2020**, *26*, 601-605.

[31] J. Cerezo, F. Santoro, *J. Comput. Chem.* **2023**, *44*,626-643.

[32] A. Humeniuk, M. Bužančić, J. Hoche, J. Cerezo, R. Mitrić, F. Santoro, V. Bonačić-Koutecký, *J. Chem. Phys.* **2020**, *152*, 057107.

[33] L. Lv, K. Yuan, T. Zhao, H. Li, Y. Wang, *ACS Omega* **2022**, *7*, 7380-7392.

[34] M. R. Craig, M. G. Hutchings, T. D. W. Claridge, H. L. Anderson, *Angew. Int. Ed.* **2001**, *40*, 1071-1074.

[35] V. Aucagne, K.D. Hanni, D.A. Leigh, P.J. Lusby, D.B. Walker, *J. Am. Chem. Soc.* **2006**, *128*, 2186-2187.

[36] Deposition numbers 2226572 (for **10**), 2226573 (for **3**), and 2226574 (for **4**) contain the supplementary crystallographic data for this paper. These data are provided free of charge by the joint Cambridge Crystallographic Data Centre and Fachinformationszentrum Karlsruhe Access Structures service.

[37] N. Demas, G. A. Crosby, *J. Phys. Chem.*, **1971**, *75*, 991-1024.

[38] M. Schmittel, G. Morbach, B. Engelen, M. Panthöferb, *CrystEngComm*, **2001**, *3*, 137-140.

[39] C. Y. K. Chan, J. W. Y. Lam, C. K. W. Jim, H. H. Y. Sung, I. D. Williams, B. Z. Tang, *Macromolecules*, **2013**, *46*, 9494-9506.

[40] L. Wang, J.-W. Wang, A.-J. Cui, X.-X. Cai, Y. Wan, Q. Chen, M.-Y. He, W. Zhang, *RSC Adv.*, **2013**, *3*, 9219-9222.

[41] W. Ren, H. Xiang, C. Peng, Z. Musha, J. Chen, X. Li, R. Huang, Y. Hu, *RSC Adv.*, **2018**, *8*, 5542-5549.

[42] J. Hu, Z. He, Z. Wang, X. Li, J. You, G. Gao, *Tetrahedron Lett.*, **2013**, *54*, 4167-4170.

[43] M. J. Frisch, G. W. Trucks, H. B. Schlegel, G. E. Scuseria, M. A. Robb, J. R. Cheeseman, G. Scalmani, V. Barone, G. A. Petersson, H. Nakatsuji, X. Li, M. Caricato, A. V. Marenich, J. Bloino, B. G. Janesko, R. Gomperts, B. Mennucci, H. P. Hratchian, J. V. Ortiz, A. F. Izmaylov, J. L. Sonnenberg, D. Williams-Young, F. Ding, F. Lipparini, F. Egidi, J. Goings, B. Peng, A. Petrone, T. Henderson, D. Ranasinghe, V. G. Zakrzewski, J. Gao, N. Rega, G. Zheng, W. Liang, M. Hada, M. Ehara, K. Toyota, R. Fukuda, J. Hasegawa, M. Ishida, T. Nakajima, Y. Honda, O. Kitao, H. Nakai, T. Vreven, K. Throssell, Jr. J. A. Montgomery, J. E. Peralta, F. Ogliaro, M. J. Bearpark, J. J. Heyd, E. N. Brothers, K. N. Kudin, V. N. Staroverov, T. A. Keith, R. Kobayashi, J. Normand, K. Raghavachari, A. P. Rendell, J. C. Burant, S. S. Iyengar, J. Tomasi, M. Cossi, J. M. Millam, M. Klene, C. Adamo, R. Cammi, J. W. Ochterski, R. L. Martin, K. Morokuma, O. Farkas, J. B. Foresman, D. J. Fox, Gaussian 16 Rev. A.03. **2016**.

[44] C. Adamo, V. Barone, *J. Chem. Phys.*, **1999**, *110*, 6158–6170.

[45] G. Scalmani, M. J. Frisch, *J. Chem. Phys.*, **2010**, *132*, 114110.

[46] R.Cammi, B. Mennucci, *J. Chem. Phys.*, **1999**, *110*, 9877− 9886.

[47] A. D. Becke, *J. Chem. Phys.*, **1993**, *98*, 5648–5652.

[48] T. Yanai, D. Tew, N. Handy, *Chem. Phys. Lett.*, **2004**, *393*, 51-57.

[49] J. Cerezo, F. Santoro, *J. Comput. Chem.*, **2022**, *44*, 626–643.